Mon. Not. R. Astron. Soc. **000**, 000–000 (0000) Printed 28 March 2016 (MN LATEX style file v2.2)

Fingers-of-God effect of infalling satellite galaxies

Chiaki Hikage[1,2], Kazuhiro Yamamoto [3]
[1] *Kavli Institute for the Physics and Mathematics of the Universe (Kavli IPMU, WPI), University of Tokyo, 5-1-5 Kashiwanoha, Kashiwa, Chiba, 277-8583, Japan*
[2] *Kobayashi-Maskawa Institute for the Origin of Particles and the Universe (KMI), Nagoya University, 464-8602, Japan*
[3] *Department of Physical Sciences, Hiroshima University, Higashi-hiroshima, Kagamiyama 1-3-1, 739-8526, Japan*

28 March 2016

ABSTRACT
Nonlinear redshift-space distortion known as the Fingers-of-God (FoG) effect is a major systematic uncertainty in redshift-space distortion studies conducted to test gravity models. The FoG effect has been usually attributed to the random motion of galaxies inside their clusters. When the internal galaxy motion is not well virialized, however, the coherent infalling motion toward the cluster center generates the FoG effect. Here we derive an analytical model of the satellite velocity distribution due to the infall motion combined with the random motion. We show that the velocity distribution becomes far from Maxwellian when the infalling motion is dominant. We use simulated subhalo catalogs to find that the contribution of infall motion is important to massive subhalos and that the velocity distribution has a top-hat like shape as expected from our analytic model. We also study the FoG effect due to infall motion on the redshift-space power spectrum. Using simulated mock samples of luminous red galaxies constructed from halos and massive subhalos in N-body simulations, we show that the redshift-space power spectra can differ from expectations when the infall motion is ignored.

Key words: cosmology: dark energy – large-scale structure of Universe – galaxies: kinematics and dynamics

1 INTRODUCTION

The peculiar motion of galaxies imprinted on redshift-space clustering provides a good probe of the dynamics of galaxies. The coherent motion of galaxies associated with gravitational evolution squashes the spatial distribution of galaxies along the line-of-sight direction, which is known as the Kaiser effect (Kaiser 1987; Hamilton 1992) and provides a unique probe of the growth rate (Peacock et al. 2001). The growth rate has been measured from the results of a variety of galaxy surveys to test general relativity and modified gravity (e.g., Yamamoto et al. 2008; Guzzo et al. 2008; de la Torre et al. 2013; Beutler et al. 2014; Reid et al. 2014). One can expect further precise measurement of the growth rate in a wide range of redshifts from the results of future cosmological surveys such as Subaru/PFS (Takada et al. 2014), Euclid (Laureijs et al. 2011), DESI (Levi et al. 2013) and WFIRST (Spergel et al. 2015).

The internal motions of galaxies in their host halos elongate the distribution of galaxies along the line-of-sight direction, which is called the Fingers-of-God (FoG) effect (Jackson 1972). The FoG effect depends on the type of galaxy (Zehavi et al. 2005). For red galaxy samples, such as luminous red galaxies (LRGs), the FoG effect is influential at scales larger than $10h^{-1}$ Mpc and can introduce serious systematics in the measurement of the cosmic growth rate (e.g., Hikage & Yamamoto 2013; Beutler et al. 2014; Reid et al. 2014). Clustering anisotropy can generally be expanded with a series of multipole power spectra $P_l(k)$ (Yamamoto et al. 2006). The Kaiser effect mainly generates quadrupole anisotropy (Kaiser 1987). Meanwhile, the FoG effect generates higher multipole anisotropy, such as hexadecapole ($l = 4$) and tetra-hexadecapole ($l = 6$) components, where the Kaiser effect is subdominant (Hikage & Yamamoto 2013). These multipoles are useful in eliminating the FoG uncertainty and provide kinematic information of satellite galaxies (Hikage 2014; Kanemaru et al. 2015).

The FoG effect is related to the kinematics of central and satellite galaxies inside their host halos. The satellite dynamics can be altered by different physical processes such as dynamical friction (Chandrasekhar 1943), tidal stripping/disruption (e.g., Boylan-Kolchin et al. 2008; Wetzel & White 2010), satellite merging, and hydrodynamical drag, such as ram pressure (Gunn & Gott 1972). Such complicated processes of satellite kinematics introduce systematic uncertainties in the determination of the dynamical mass of galaxy clusters through satellite velocity dispersion (e.g., Wu et al. 2013). The velocity distribution of satellites has been studied by conducting various numerical simulations (e.g., Ghigna et al. 2000; Diemand et al. 2004; Faltenbacher et al. 2005; Wu et al. 2013). A non-zero velocity of central galaxies relative to the host halo has been found in several studies (e.g., van den Bosch et al. 2005; Guo et al. 2015).

The FoG effect has usually been attributed to the random motion of galaxies inside clusters or halos. Meanwhile, coherent infall motion onto the halo mass center also generates the FoG effect, as illustrated by Hamilton (1992). The infall region of clusters forming a trumpet-shaped pattern has been observed for a number of

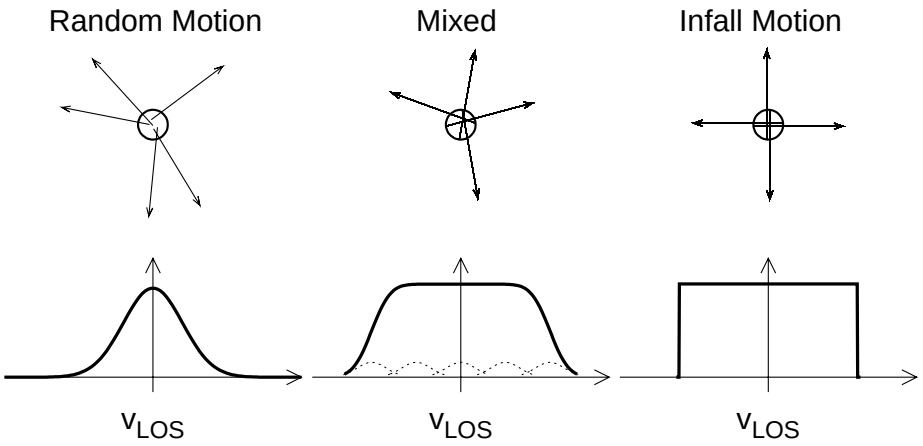

Figure 1. Illustration of the line-of-sight velocity distribution $v_{\rm LOS}$ due to random motion (left), coherent infall motion (right) and their combination (center). The velocity distribution due to coherent infall motion has a top-hat shape, while the random motion produces a Gaussian velocity distribution.

clusters and provides an important probe of the cluster mass profile insensitive to the details of galaxy formation (Regos & Geller 1989; Diaferio & Geller 1997; Rines et al. 2003; Zu & Weinberg 2013). In this letter, we study the FoG effect due to the infall motion of satellites on the redshift-space power spectrum. We derive a theoretical model of the line-of-sight velocity distribution due to the random and infall motions of satellites inside their halos. We use simulated subhalo catalogs to test our model expectations and to study the effect on the redshift-space power spectra. Here we focus on LRGs that have been widely used in cosmological studies (e.g., Reid et al. 2010; Beutler et al. 2014; Reid et al. 2014). Although the satellite fraction of LRGs is only about 6%, the effects of the satellite FoG effect on the growth rate measurement have been found to be large (Hikage & Yamamoto 2013). Understanding the behavior of satellite motion is important in precise cosmological studies using redshift-space power spectra of LRG samples.

This letter is organized as follows. In section 2, we model satellite internal motion by decomposing the infall and randomly rotating components. The details of our simulations are explained in section 3. In section 4, we present results, comparing the satellite velocity distribution with the theoretical modeling derived in section 2, and evaluate the FoG effects of the infall velocity and random velocity on redshift-space galaxy clustering. Section 5 summarizes the letter and presents conclusions.

2 SATELLITE MOTION INSIDE HOST HALOS

The internal satellite velocity with respect to the host halo bulk velocity $\mathbf{v}_{\rm sat} \equiv \mathbf{V}_{\rm sat} - \mathbf{V}_{\rm halo}$ can be decomposed into a component infalling onto the halo center and a tangential component:

$$\mathbf{v}_{\rm sat} = (-\langle v_{\rm inf}\rangle + \epsilon_{\rm inf})\mathbf{e}_r + \epsilon_{{\rm tan},\theta}\mathbf{e}_\theta + \epsilon_{{\rm tan},\phi}\mathbf{e}_\phi, \quad (1)$$

where the mean infall velocity $\langle v_{\rm inf}\rangle$ is generally non-zero and defined to have a positive sign in the direction toward the halo center. The average velocity dispersions in the infall and tangential directions are defined as $\sigma^2_{\rm v,inf} \equiv \left\langle \epsilon^2_{\rm inf}\right\rangle$ and $\sigma^2_{\rm v,tan} \equiv \left\langle \epsilon^2_{{\rm tan},\theta}\right\rangle = \left\langle \epsilon^2_{{\rm tan},\phi}\right\rangle$ respectively, and depend on the host halo mass M. The line-of-sight (one-dimensional) component of the internal satellite velocity $v_{\rm LOS} \equiv \mathbf{v}_{\rm sat}\cdot\mathbf{e}_{\rm LOS}$ becomes

$$v_{\rm LOS} = (-\langle v_{\rm inf}\rangle + \epsilon_{\rm inf})\mu + \epsilon_{{\rm tan},\theta}(1-\mu^2)^{1/2}, \quad (2)$$

where μ is the cosine of the angle between the line of sight and the direction of infall toward the halo center; i.e., $\mu \equiv \mathbf{e}_r\cdot\mathbf{e}_{\rm LOS}$. When the infall and tangential velocities are given by independent Gaussian distributions, the line-of-sight velocity distribution of satellites in the direction of μ becomes a Gaussian distribution with a mean of $-\mu\langle v_{\rm inf}\rangle$ and variance of

$$\sigma^2_{{\rm v},\mu}(\mu;M) = \mu^2\sigma^2_{\rm v,inf}(M) + (1-\mu^2)\sigma^2_{\rm v,tan}(M). \quad (3)$$

The line-of-sight velocity distribution averaged over μ is given by

$$f_{\rm v}(v_{\rm LOS};M) = \frac{1}{2}\int_{-1}^{1} d\mu \frac{1}{(2\pi)^{1/2}\sigma_{{\rm v},\mu}(\mu;M)} \times \exp\left[-\frac{(v_{\rm LOS}+\mu\langle v_{\rm inf}\rangle(M))^2}{2\sigma^2_{{\rm v},\mu}(\mu;M)}\right]. \quad (4)$$

The velocity dispersion of satellites is the second moment of the equation (4) and becomes

$$\sigma^2_{\rm v,LOS}(M) = \frac{1}{3}(\langle v_{\rm inf}\rangle^2 + \sigma^2_{\rm v,inf} + 2\sigma^2_{\rm v,tan}). \quad (5)$$

When the internal motion of galaxies is well virialized, the mean infall velocity is negligible compared with the random motion and the internal velocity distribution is isotropic, i.e., $\sigma_{\rm v,inf} = \sigma_{\rm v,tan} = \sigma_{\rm vir}$, where $\sigma_{\rm vir}$ is the virial velocity dispersion. Equation (4) simply becomes the Gaussian distribution

$$f_v(v_{\rm LOS};M) = \frac{1}{(2\pi)^{1/2}\sigma^2_{\rm v,vir}}\exp\left[-\frac{v^2_{\rm vir}}{2\sigma^2_{\rm v,vir}}\right], \quad (6)$$

which is illustrated in the left panel of Figure 1. Meanwhile, when the mean infall velocity is dominant ($\langle v_{\rm inf}\rangle \gg \sigma_{\rm v,inf}, \sigma_{\rm v,tan}$), equation (4) becomes a top-hat distribution:

$$f_v(v_{\rm LOS};M) = \begin{cases} 0.5\langle v_{\rm inf}\rangle^{-1} & (|v_{\rm LOS}| \leqslant \langle v_{\rm inf}\rangle) \\ 0 & (|v_{\rm LOS}| > \langle v_{\rm inf}\rangle) \end{cases}, \quad (7)$$

where the line-of-sight velocity dispersion becomes $\sigma_{\rm v,LOS} = \langle v_{\rm inf}\rangle/\sqrt{3}$ (see the right panel in Figure 1). In reality, the infall motion and random motion combine and the line-of-sight velocity distribution is then described by the sum of Gaussian distributions with different mean values of $\mu\langle v_{\rm inf}\rangle$ in the range of μ from -1 to 1. The shape of the distribution then becomes a smoothed top-hat function like that seen in the center panel of Figure 1.

3 SIMULATIONS

To validate our modeling of the line-of-sight velocity distribution derived in the previous section, we construct subhalo catalogs from

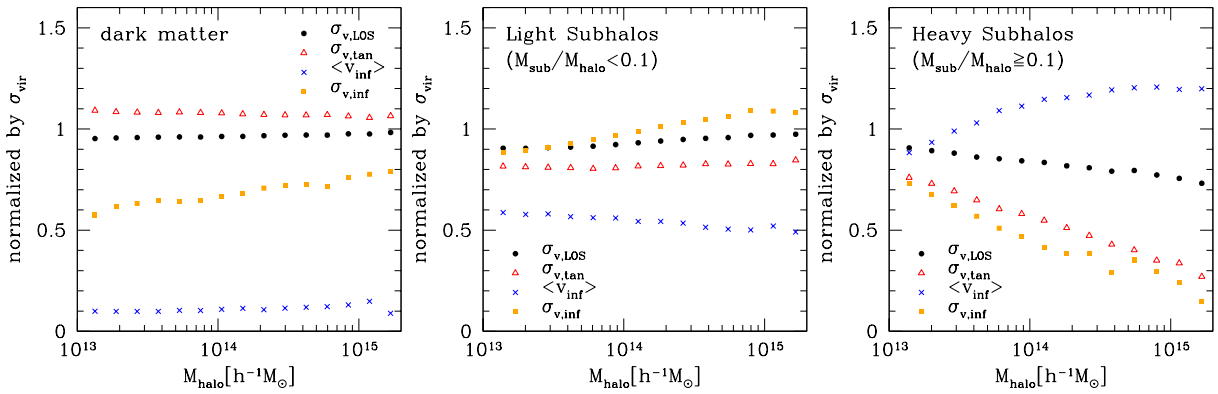

Figure 2. Halo mass dependence of the line-of-sight (one-dimensional) velocity dispersion $\sigma_{\rm v,LOS}$ (black circles), radial and tangential velocity dispersions $\sigma_{\rm v,inf}$ (yellow square) and $\sigma_{\rm v,tan}$ (red triangle) and mean infall velocity $\langle v_{\rm inf}\rangle$ (blue crosses) relative to the virial velocity dispersion $\sigma_{\rm vir}$.

N-body simulations. We make 10 realizations using GADGET-2 public code (Springel 2005), starting from an initial redshift of 80 and a 2LPT initial condition (Crocce et al. 2006). The side length of the simulation box is $600h^{-1}$ Mpc and the number of particles is 800^3, which corresponds to a particle mass of $2.8\times10^{10}h^{-1}M_\odot$. The softening length is set to $10h^{-1}$ kpc. We compute the initial power spectrum using CAMB software (Lewis et al. 2000) by assuming a flat ΛCDM cosmology with the parameters $\Omega_m = 0.273$, $\Omega_b = 0.046$, $h = 0.704$, $n_s = 0.963$, $\tau = 0.089$, and $\sigma_8 = 0.809$. We use snapshot data at $z = 0.3$ roughly corresponding to the mean redshift of the LRG sample of the Sloan Digital Sky Survey (SDSS) (Eisenstein et al. 2001). Halos are identified using the friends-of-friends algorithm with a linking length $b = 0.2$ and setting the minimum number of particles for halos to 32. Subhalos are identified using the SUBFIND code (Springel et al. 2001) with the minimum number of particles set to 20. We take the z-axis as the line-of-sight direction to add the peculiar velocity effect as $r \to r + (1+z)v_z/aH(z)$.

We describe the relationship between halos and galaxies using the halo occupation distribution (HOD) (Kravtsov et al. 2004; Zehavi et al. 2005; White et al. 2011). We use a conventional HOD form with five parameters (Zheng et al. 2005):

$$\langle N_{\rm cen}(M)\rangle = \frac{1}{2}\left[1+{\rm erf}\left(\frac{\log_{10}(M)-\log_{10}(M_{\rm min})}{\sigma_{\log M}}\right)\right] \quad (8)$$

$$\langle N_{\rm sat}(M)\rangle = \langle N_{\rm cen}\rangle\left(\frac{M-M_{\rm cut}}{M_1}\right)^{\alpha}, \quad (9)$$

where ${\rm erf}(x)$ is the error function. We fix the HOD values for an SDSS LRG as (Reid & Spergel 2009) $M_{\rm min} = 5.7\times10^{13}h^{-1}M_\odot$, $\sigma_{\log M} = 0.7$, $M_{\rm cut} = 3.5\times10^{13}h^{-1}M_\odot$, $M_1 = 3.5\times10^{14}h^{-1}M_\odot$, and $\alpha = 1$. The position of the central galaxy is assigned to be the potential minimum of the halo and the velocity is assigned as the mean of all dark matter particles inside central subhalos. We use three different types of tracers for satellite galaxies; one type is randomly selected dark matter particles and the others are subhalos with mass relative to the host halo mass $f_{\rm sub} \equiv M_{\rm sub}/M_{\rm halo}$ of <0.1 and $\geqslant 0.1$ (hereafter referred to as "light subhalos" and "heavy subhalos" respectively).

4 RESULTS

4.1 Satellite velocity distribution

We use simulated subhalo catalogs and decompose the internal velocity of satellites relative to the host halo velocity into infall and tangential velocity components. Figure 2 shows the results of the host halo mass dependence of each velocity component: the line-of-sight velocity dispersion $\sigma_{\rm v,LOS}$, mean infall velocity $\langle v_{\rm inf}\rangle$ and the infall and tangential velocity dispersion $\sigma_{\rm v,inf}$ and $\sigma_{\rm v,tan}$. The panels show the result when satellites are represented using dark matter particles, light subhalos, and heavy subhalos from left to right. Each velocity component is normalized with the virial velocity dispersion $\sigma_{\rm vir}$ for the corresponding host halo mass.

When satellites are represented by dark matter particles, the mean infall velocity is low and the line-of-sight velocity dispersion is nearly equal to the virial velocity dispersion. This indicates that the motion of dark matter particles is well virialized. Meanwhile, the motion of subhalos is quite different from that of dark matter particles. The mean infall velocity of subhalos is much higher than that of the dark matter particles and it is comparable to the virial velocity for massive subhalos. The tangential velocity reduces as the mean infall velocity increases. This indicates that the dynamical friction becomes efficient for heavier subhalos and the orbital motion slows down. The velocity bias of the line-of-sight velocity dispersion varies depending on the host halo mass and the subhalo mass. Our result shows that the line-of-sight velocity dispersion is smaller than the virial velocity dispersion. The result may change quantitatively when the subhalo finders are different. The inner fast rotating subhalos are difficult to identify using the SUBFIND algorithm and the average velocity of satellite subhalos is thus lower than that in previous works (e.g., Diemand et al. 2004). The qualitative result that the infall motion is dominant in heavier subhalos is consistent with the results obtained previously.

Figure 3 shows the line-of-sight velocity distribution of satellites represented by dark matter particles (left), light subhalos (center) and heavy subhalos (right) for different bins of host halo mass. The velocity distribution for dark matter satellites agrees with a Gaussian distribution with virial velocity dispersion for each bin of the halo mass. For satellite subhalos, the mean infall velocity is comparable to or larger than the tangential velocity. The resulting shape of the line-of-sight velocity distribution does not become a simple Gaussian but has a more top-hat-like shape, particularly for heavy subhalos. This feature is consistent with previous results obtained by Diemand et al. (2004), who pointed out that the subhalo velocity distribution becomes non-Maxwellian. We compare the simulation results with our modeling using the simulated values of the mean infall velocity and velocity dispersions. For heavy subhalos (the right panel of Figure 3), our modeling of the line-of-sight

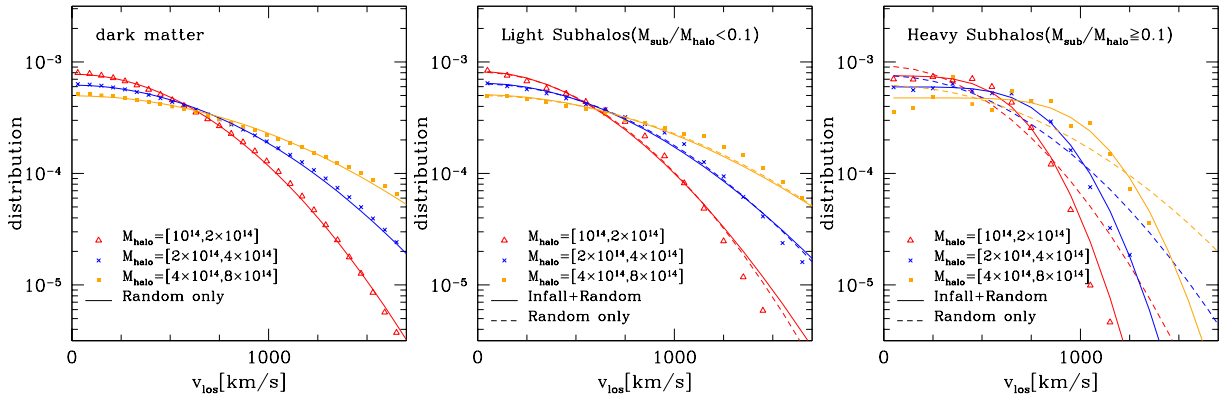

Figure 3. Distribution function of the line-of-sight velocity $v_{\rm los}$ distribution of satellites for three different ranges of halo mass from $10^{14}h^{-1}M_\odot$ to $8\times10^{14}h^{-1}M_\odot$. Satellites are represented with dark matter particles (left), light subhalos (center) and heavy subhalos (right). Reference lines are a Gaussian distribution of the one-dimensional velocity dispersion (eq. [6], dashed) and our velocity model including both the infall and random motions (eq. [4], solid).

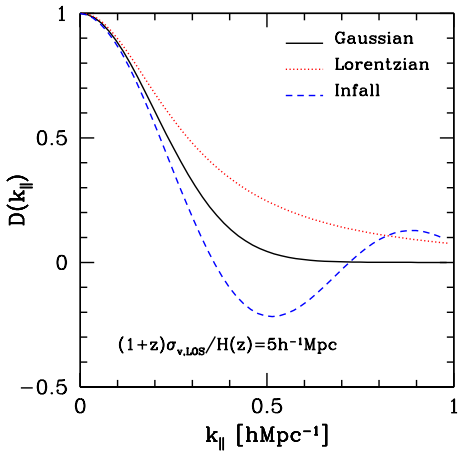

Figure 4. Comparison of the FoG damping function $\mathcal{D}(k_\parallel)$ (eq. [10]) when the infall motion or random motion is dominant. For comparison, we plot the Lorentzian form of FoG damping. The velocity dispersion $\sigma_{\rm v,LOS}/aH(a)$ is set to $5h^{-1}$ Mpc.

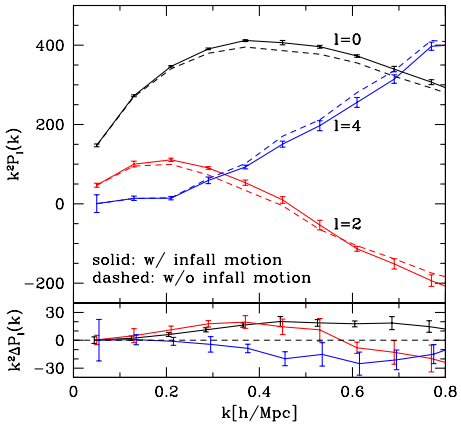

Figure 5. Mock LRG power spectra P_l simulated with the halo model description. Satellites are represented by massive subhalos (where the average ratio of the subhalo mass to the host halo mass is 0.06) and the satellite fraction is about 6.4%. For comparison, we plot the power spectra where the velocity of satellite subhalos is rotated randomly.

velocity distribution given by equation (4) describes the simulation results better than a simple Gaussian distribution (eq. [6]).

4.2 FoG effect on the redshift-space power spectrum

Satellite motion inside halos generates non-linear redshift-space distortion, often referred as the FoG effect. The FoG effect on multipole components of the redshift-space power spectrum is formulated employing the halo model (e.g., Hikage et al. 2013; Hikage & Yamamoto 2013). FoG damping due to internal satellite motion of the halo with mass M is given by Fourier transforming the line-of-sight velocity distribution of satellites:

$$\mathcal{D}(k_\parallel;M)=\int dv f_v(v;M)\exp(-i\tilde{k}_\parallel v)$$
$$\simeq\exp\left[-\frac{\tilde{k}_\parallel^2(\sigma_{\rm v,sat}^2-\langle v_{\rm inf}\rangle^2/3)}{2}\right]\frac{\sin(\tilde{k}_\parallel\langle v_{\rm inf}\rangle)}{\tilde{k}_\parallel\langle v_{\rm inf}\rangle}, \quad (10)$$

where $\tilde{k}=(1+z)k_\parallel/H(z)$ and $k_\parallel$ is the line-of-sight component of the wavevector $\mathbf{k}$. In the second line, we make the approximation that $\sigma_{\rm v,inf}\simeq\sigma_{\rm v,tan}$. Figure 4 compares the FoG damping function in different cases. When the mean infall velocity is equal to zero, FoG damping has a simple Gaussian form. When the infall velocity is dominant, the velocity distribution has a top-hat form and its Fourier-transform is a sinc function, as shown by the dashed line in Figure 4. FoG damping due to the infall motion has a shape quite different from the commonly used Gaussian or Lorentzian form and affects the small-scale features of redshift-space clustering.

Figure 5 shows the multipole power spectra $k^2P_l(k)$ ($l=0,2,4$ from left to right) of simulated samples assuming the HOD of SDSS LRGs. Satellites in the samples are represented by heavy subhalos, which is a good assumption because LRGs are massive galaxies and thus should have massive host subhalos. The average ratio of the subhalo mass to the host halo mass becomes 6.4%. In this sample, the mean infall velocity is comparable to the virial velocity of satellite-hosting halos and the values of each velocity component of satellite subhalos are $\langle v_{\rm inf}\rangle=0.79\sigma_{\rm vir}$; $\sigma_{\rm v,inf}=0.95\sigma_{\rm vir}$; $\sigma_{\rm v,tan}=0.86\sigma_{\rm vir}$. To see the effect of coherent infall motion, we also plot the power spectra of the same mock samples where the direction of the internal satellite velocity

$\mathbf{v}_{\rm sat}$ is randomly rotated to erase the coherent infall motion while the absolute value $|\mathbf{v}_{\rm sat}|$ is the same. The error bars represent the 1-sigma scatter of the power spectra P_l for 10 LRG mock samples divided by the square root of 10. Assuming that the sample variance is proportional to the survey volume, the plotted error corresponds to the statistical error for the survey with the sample volume of $2.16h^{-3}{\rm Gpc}^3$ ($=10\times(600h^{-1}{\rm Mpc})^3$), which is roughly the same volume as for the BOSS/CMASS sample (Beutler et al. 2014). The effect of the infalling motion of satellites becomes appreciable on smaller scales ($k\gtrsim 0.2h{\rm Mpc}^{-1}$) because the internal velocity distribution is sensitive to the small-scale power spectrum via the FoG effect. We evaluate the effect of the infall FoG on the overall shape of multipole power spectra as chi-square values:

$$\chi^2\equiv\sum_{l}^{0,2,4}\sum_{i}^{k_i<k_{\rm max}}\frac{[P_l^{\rm w/infall}(k_i)-P_l^{\rm w/o\ infall}(k_i)]^2}{\sigma_{P_l}^2(k_i)}, \qquad (11)$$

where σ_{P_l} is the 1σ error of P_l for the survey with $2.16h^{-3}$ Gpc^3 volume, and $k_{\rm max}$ is the maximum value of k for the χ^2 calculation. The binning width of k for the χ^2 calculation is set to be $0.04h{\rm Mpc}^{-1}$. The chi-square value increases at larger $k_{\rm max}$: $\chi^2=10$ at $k_{\rm max}=0.21h{\rm Mpc}^{-1}$, $\chi^2=89$ at $k_{\rm max}=0.29h{\rm Mpc}^{-1}$, and $\chi^2=190$ at $k_{\rm max}<0.41h{\rm Mpc}^{-1}$. Our result indicates that the proper treatment of the infall FoG would be necessary for the precise modeling of redshift-space power spectra for massive galaxies such as LRGs at $k\gtrsim 0.2h{\rm Mpc}^{-1}$.

5 SUMMARY AND CONCLUSIONS

We investigated satellite motion inside host halos and the resulting FoG effect on the power spectrum. When the satellite motion is not well virialized, the internal satellite motion is not random but has coherent infalling flow onto the halo center. We used subhalo catalogs to find that the infall motion becomes important when the subhalo mass relative to the host halo mass increases and the line-of-sight velocity distribution then deviates from Maxwellian and has a flat top-hat form. We derived a theoretical model of the satellite velocity including both infall and random motions. We found that our model well describes the simulated subhalo velocity distribution. We also investigated how the difference in the velocity structure between random motion and infall motion affects the shape of redshift-space power spectra. We showed that the effect of infall motion on the overall shape of an LRG-like power spectrum is appreciable on the scale $k>0.2h$ per Mpc for the current survey volume, such as the BOSS/CMASS sample volume.

The effect of infall motion may be important in precision cosmological studies using redshift-space galaxy clustering in future surveys such as Subaru/PFS, DESI, Euclid, and WFIRST. We found that the contribution of infall motion depends on the mass of subhalos hosting satellites. Galaxy–galaxy lensing provides the information of subhalo mass hosting satellite galaxies (e.g., Li et al. 2014). It would be interesting to see how the galaxy–galaxy lensing measurement from the upcoming imaging and redshift surveys can remove the uncertainty of the infall motion effect. We leave this as a topic of research to be addressed in the near future.

ACKNOWLEDGMENTS

We thank Takahiko Matsubara for useful discussions. This work was supported by MEXT/JSPS KAKENHI Grant Numbers 24740160 and 15H05895.

REFERENCES

Beutler F. et al., 2014, MNRAS, 443, 1065
Boylan-Kolchin M., Ma C.-P., Quataert E., 2008, MNRAS, 383, 93
Chandrasekhar S., 1943, ApJ, 97, 255
Crocce M., Pueblas S., Scoccimarro R., 2006, MNRAS, 373, 369
de la Torre S. et al., 2013, A.&Ap., 557, A54
Diaferio A., Geller M. J., 1997, ApJ, 481, 633
Diemand J., Moore B., Stadel J., 2004, MNRAS, 352, 535
Eisenstein D. J. et al., 2001, AJ, 122, 2267
Faltenbacher A., Kravtsov A. V., Nagai D., Gottlöber S., 2005, MNRAS, 358, 139
Ghigna S., Moore B., Governato F., Lake G., Quinn T., Stadel J., 2000, ApJ, 544, 616
Gunn J. E., Gott, III J. R., 1972, ApJ, 176, 1
Guo H. et al., 2015, MNRAS, 446, 578
Guzzo L., et al., 2008, Nature, 451, 541
Hamilton A. J. S., 1992, ApJ, 385, L5
Hikage C., 2014, MNRAS, 441, L21
Hikage C., Mandelbaum R., Takada M., Spergel D. N., 2013, MNRAS, 435, 2345
Hikage C., Yamamoto K., 2013, JCAP, 8, 19
Jackson J. C., 1972, MNRAS, 156, 1P
Kaiser N., 1987, MNRAS, 227, 1
Kanemaru T., Hikage C., Hütsi G., Terukina A., Yamamoto K., 2015, Phys. Rev. D, 92, 023523
Kravtsov A. V., Berlind A. A., Wechsler R. H., Klypin A. A., Gottlöber S., Allgood B., Primack J. R., 2004, ApJ, 609, 35
Laureijs R. et al., 2011, ArXiv e-prints (arXiv:1110.3193)
Levi M. et al., 2013, ArXiv e-prints (arXiv:1308.0847)
Lewis A., Challinor A., Lasenby A., 2000, ApJ, 538, 473
Li R. et al., 2014, MNRAS, 438, 2864
Peacock J. A., et al., 2001, Nature, 410, 169
Regos E., Geller M. J., 1989, AJ, 98, 755
Reid B. A. et al., 2010, MNRAS, 404, 60
Reid B. A., Seo H.-J., Leauthaud A., Tinker J. L., White M., 2014, MNRAS, 444, 476
Reid B. A., Spergel D. N., 2009, ApJ, 698, 143
Rines K., Geller M. J., Kurtz M. J., Diaferio A., 2003, AJ, 126, 2152
Spergel D. et al., 2015, ArXiv e-prints (arXiv:1503.03757)
Springel V., 2005, MNRAS, 364, 1105
Springel V., Yoshida N., White S. D. M., 2001, Nature, 6, 79
Takada M. et al., 2014, PASJ, 66, 1
van den Bosch F. C., Weinmann S. M., Yang X., Mo H. J., Li C., Jing Y. P., 2005, MNRAS, 361, 1203
Wetzel A. R., White M., 2010, MNRAS, 403, 1072
White M. et al., 2011, ApJ, 728, 126
Wu H.-Y., Hahn O., Evrard A. E., Wechsler R. H., Dolag K., 2013, MNRAS, 436, 460
Yamamoto K., Nakamichi M., Kamino A., Bassett B. A., Nishioka H., 2006, PASJ, 58, 93
Yamamoto K., Sato T., Hütsi G., 2008, Progress of Theoretical Physics, 120, 609
Zehavi I. et al., 2005, ApJ, 630, 1
Zheng Z., et al., 2005, ApJ, 633, 791
Zu Y., Weinberg D. H., 2013, MNRAS, 431, 3319